Neuron
Article

Rat Olfactory Bulb Mitral Cells Receive Sparse Glomerular Inputs

Antoniu L. Fantana,[1,2] Edward R. Soucy,[1] and Markus Meister[1,*]
[1]Molecular and Cellular Biology Department and Center for Brain Science
[2]Program in Neuroscience
Harvard University, Cambridge, MA 02138, USA
*Correspondence: meister@fas.harvard.edu
DOI 10.1016/j.neuron.2008.07.039

SUMMARY

Center-surround receptive fields are a fundamental unit of brain organization. It has been proposed that olfactory bulb mitral cells exhibit this functional circuitry, with excitation from one glomerulus and inhibition from a broad field of glomeruli within reach of the lateral dendrites. We investigated this hypothesis using a combination of in vivo intrinsic imaging, single-unit recording, and a large panel of odors. Assuming a broad inhibitory field, a mitral cell would be influenced by >100 contiguous glomeruli and should respond to many odors. Instead, the observed response rate was an order of magnitude lower. A quantitative model indicates that mitral cell responses can be explained by just a handful of glomeruli. These glomeruli are spatially dispersed on the bulb and represent a broad range of odor sensitivities. We conclude that mitral cells do not have center-surround receptive fields. Instead, each mitral cell performs a specific computation combining a small and diverse set of glomerular inputs.

INTRODUCTION

Lateral inhibition is a prominent motif in many neuronal circuits, in which each neuron receives inhibition from the output of other cells in the same population. Sometimes, the field of lateral connections is broad and dense, collecting input from every neuron within some range. Classic examples are the inhibitory fields of photoreceptors (Hartline et al., 1956), bipolar cells (Werblin and Dowling, 1969), and ganglion cells (Kuffler, 1953) in the retina. In other cases, the lateral interactions are rather sparse and specific, for example the horizontal connections in visual cortex (Sincich and Blasdel, 2001; Yoshioka et al., 1996). The computational role of these two arrangements is likely different: dense lateral inhibition in the retina can serve to enhance local stimulus differences and suppress broadly correlated input (Ratliff and Hartline, 1959; Srinivasan et al., 1982). By comparison, sparse lateral connectivity likely serves more specific computations involving select features, such as crossorientation suppression (Olshausen and Field, 2005; Sincich and Blasdel, 2001). Which of these scenarios applies in the olfactory bulb?

Receptor neurons in the olfactory epithelium send their axons to terminate in discrete glomeruli on the surface of the olfactory bulb (Mombaerts, 2006). Each glomerulus receives input from one or a few olfactory receptor types and thus represents a distinct channel of olfactory information. The circuits of the olfactory bulb combine signals from these input channels into the responses of mitral cells, whose axons project to downstream brain areas (Shepherd and Greer, 2004). Each mitral cell sends a single apical dendrite into a primary glomerulus, where it receives excitation from the receptor neurons. It receives inhibition from interneurons in the glomerular layer, originating both locally and in distant glomeruli (Aungst et al., 2003; Wachowiak and Shipley, 2006). The mitral cell also extends a broad field of lateral dendrites that form reciprocal synapses with granule cells (Isaacson and Strowbridge, 1998; Egger and Urban, 2006). By this route, a mitral cell receives disynaptic inhibition from other mitral cells (Figure 1A), and given the anatomical extent of the lateral dendrites, this inhibitory influence might derive from a dense field with many hundreds of glomeruli (Figure 1B). Indeed, a prior study concluded in favor of this view (Luo and Katz, 2001).

Here, we investigate the functional extent of these lateral interactions. Which of the many glomeruli actually influence a mitral cell's firing? Following prior usage, we will call this set of glomeruli the mitral cell's "receptive field" (Luo and Katz, 2001). To probe the structure of this receptive field, we used a large panel of odors to activate the glomeruli in many possible patterns and monitored these input patterns by optical imaging. We also recorded the firing of mitral cells under the same stimuli and devised a response analysis that could detect any change in firing pattern with high sensitivity. It emerged that the firing of a typical mitral cell is governed by just a few glomeruli (Figure 1C) that are spatially dispersed and functionally diverse. Apparently, only a few of the many possible lateral connections dominate the response of a mitral cell.

RESULTS

Dynamic Firing Patterns in the Mitral Cell's Odor Response

We recorded the firing of 179 individual mitral cells in the olfactory bulb of anesthetized rats. The stimulus consisted of odor pulses delivered to the nose, 10–20 s in duration, interleaved with exposure to clean air. The animal sampled the odors through periodic inhalations, and this breathing rhythm imposes

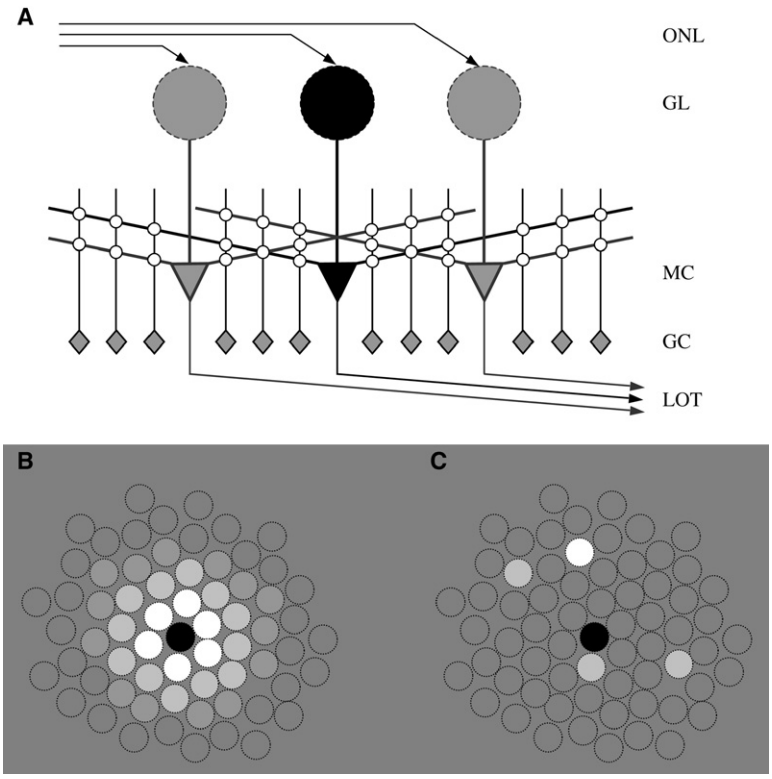

Figure 1. Functional Connectivity between Glomeruli and Mitral Cells

(A) Circuits for lateral signal flow in the external plexiform layer of the olfactory bulb. Mitral cells (MC) receive afferent inputs from receptor axons that terminate in glomeruli (GL). MCs also extend lateral dendrites horizontally over large distances. The processes of granule cells (GC) run largely vertically and form reciprocal synapses with mitral cell dendrites, where the MC excites the GC and the GC inhibits the MC. Additional circuits for lateral inhibition exist in the glomerular layer (not shown here). ONL, olfactory nerve layer; LOT, lateral olfactory tract.

(B) Dense receptive field hypothesis. In this top view of the glomerular array, a mitral cell receives strong excitation from its principal glomerulus (black) and inhibition from a dense field of surrounding glomeruli (white), declining gradually with distance in the dendritic field.

(C) Sparse receptive field hypothesis. The mitral cell receives strong input from only a few glomeruli (filled circles), while the others (open circles) have negligible influence.

a strong pattern on the firing of mitral cells (Adrian, 1942; Onoda and Mori, 1980). In the presence of an odor, the firing pattern changes (Macrides and Chorover, 1972; Chaput et al., 1992). For the present study, we required a very sensitive measure of these changes in order to resolve the influence of different glomeruli on the mitral cell's response.

The most commonly used measure of the odor response is the total number of spikes fired during an inhalation (Davison and Katz, 2007; Fletcher and Wilson, 2003; Yokoi et al., 1995). However, we observed that many odors did not affect the average firing rate but altered the distribution of spikes throughout the inhalation period (Macrides and Chorover, 1972; Chaput et al., 1992). Therefore, instead of simply counting each respiration's spikes, we chose a graphical display that indicates the position or "phase" of each spike during the respiration cycle (Figure 2).

For some neurons, the response behavior seemed to be wholly captured by changes in the firing rate (Figure 2A). Other cells however, showed very clear odor responses as judged by phase plots, without any change in the firing rate (Figures 2B, 2C, and 2E). Furthermore, two odors can produce responses with a similar change in firing rate but qualitatively distinct phase plots (Figure 2D). When the same sequence of odors was repeated, these cells produced identical firing patterns (Figures 2A–2D), indicating that the respiration-locked phase shifts are indeed reliable indicators of the odor response.

A Sensitive Measure of Mitral Cell Response Dynamics

On this background, the goal was to reliably detect subtle changes in the firing pattern as the stimulus switches from air to odor. As is apparent from the phase plots in Figure 2, the changes were usually restricted to one or a few portions of the respiration cycle, while others remained unchanged. Ideally, a weighted average would be applied to emphasize the phases that show the largest odor-related change in firing. Of course, this weighting would need to be chosen appropriately for each different neuron.

To generalize this linear weighting approach, we performed a principal component analysis (PCA) on the set of spike trains in all respiration cycles (see Experimental Procedures). This method identifies one or more linear weighting schemes that best discriminate between air and odor exposure. For most mitral cells, we found that a single principal component accounted for almost all of the explainable variance in the data set (Figure 3A). The remaining variance was dominated by stimulus-independent noise, as estimated by a shuffle test (Figure 3A and Experimental Procedures). Thus, we measured the mitral cell's response by the projection of the firing pattern onto the first principal component, computed individually for each mitral cell (Figure 3B). This yields a single scalar response number for every respiration cycle. Responses of different sign can be captured, and in general, larger changes in the firing pattern translate into larger response magnitudes (Figure 3B). Overall, this sensitive measure of mitral cell firing detected ~3-fold more odor responses than the average firing rate (Figure 4A).

At Moderate Odor Concentrations, Mitral Cell Responses Are Sparse

With this response measure in hand, we sought to identify which odors actually elicit a change in a mitral cell's firing. Since there is always some stochastic variation in firing, one needs to identify changes that significantly exceed this background noise. For this purpose, each odor presentation was divided into three segments of equal duration: the first half of the air exposure prior to the odor, the second half, and the odor exposure itself. The firing response was computed for each segment. Then we computed the response change between air and

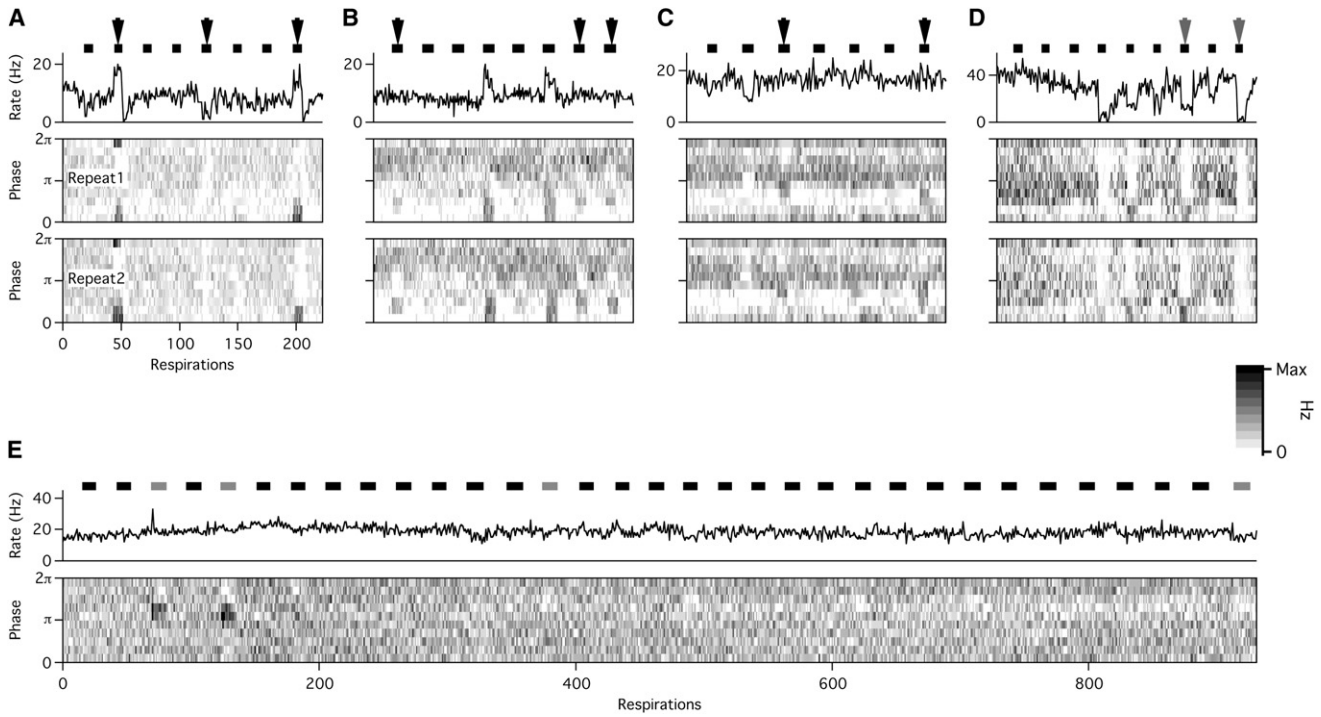

Figure 2. Dynamics of the Mitral Cell Odor Response

(A) Firing of a mitral cell under two repeats of the same odor sequence (~11 min apart). Top graph: firing rate, averaged over each respiration cycle. Black bars indicate periods of odor exposure, each using a different odorant. Middle and bottom graph: Phase plot of the spike train. Each vertical strip corresponds to one respiration cycle and denotes firing rate versus phase in the cycle, encoded by the gray scale. Arrows indicate odor responses with distinct increases or decreases in the average firing rate. Note that these also involve clear changes in the phase distribution of spikes.

(B) Firing of another sample mitral cell, displayed as in panel (A). Two repeats ~10 min apart. Arrowheads indicate odor responses with no change in the firing rate but a clear change in the phase plot.

(C) Firing of another sample mitral cell, displayed as in panel (B). Two repeats ~50 min apart.

(D) Firing of another sample cell, displayed as in panel (A). Two repeats ~12 min apart. Arrowheads indicate odor responses with similar reduction in the firing rate but different phase distribution.

(E) Firing of another sample cell under a longer odor series. Gray stimulus bars indicate responses deemed significant by the thresholds applied in Figure 4.

odor and compared that to the change between the two air presentations.

To determine which of these responses are significant, we used the receiver-operator characteristic (ROC), a method derived from signal-detection theory (Green and Swets, 1974). Briefly, one chooses a threshold above which a change in firing pattern is called significant. When applied to the air/odor comparison, this threshold will deliver a number of "hits." When applied to the air/air comparison, it produces a number of "false alarms," which are due to stochastic variations in firing. As the threshold is gradually raised from zero, the number of hits and false alarms change at different rates, yielding the ROC curve (Figure 4A). On this curve, we chose a threshold that accepts ten false alarms for every 100 hits. Note that the traditional response measure using firing rate alone would yield a much inferior ROC curve that detects 3-fold fewer hits for the same fraction of false alarms.

From an initial panel of ~200 odors, a set of 40 were selected because they prominently activate glomeruli in the dorsal olfactory bulb (see Table S2, List A). Among these 40 odors, the average mitral cell produced a significant response for only 2.0 odors (Figure 4B). Surprisingly, half of the mitral cells did not respond to any odors in the set (Figure 4B). If the mitral cell had a dense receptive field among the glomeruli, one might expect that any odor activating a glomerulus within reach of the lateral dendrites should produce a detectable change in firing. In this case, the notable lack of responses could be explained if the odor panel activated glomeruli located at a great distance from half of the recorded mitral cells, for example glomeruli clustered mainly on one side of the bulb. Alternatively, the mitral cell might have a sparse receptive field, dominated by just a few glomerular inputs.

At Moderate Odor Concentrations, Glomerular Responses Are Sparse

To interpret the influence of glomeruli on mitral cell responses, we followed the activity patterns among glomeruli under the same panel of odors. We used the method of intrinsic signal imaging. When the bulb surface is illuminated with deep red light, activated glomeruli appear as spots of decreased reflectance (Rubin and Katz, 1999; Uchida et al., 2000; Meister and Bonhoeffer, 2001). For each of the glomeruli identified this way, its activity was measured by the intensity of the spot (see Experimental Procedures). For statistical controls, a number of

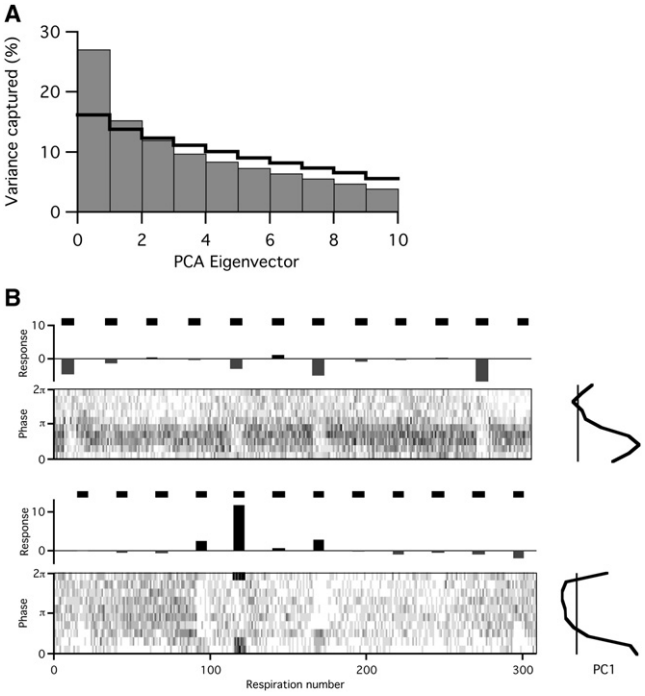

Figure 3. A Sensitive Measure of the Mitral Cell Response

(A) For each cell, the firing patterns from the phase plot were subjected to a principal components analysis (see Experimental Procedures). The graph shows how much variance in the data set was captured by the first ten PCA eigenvectors, averaged over 179 cells (gray bars). To estimate the noise variance in the data set, a shuffle test was performed (see Experimental Procedures) and the procedure repeated (black line). Only for the first component does the variance substantially exceed the expected noise level. Examples of the first component are shown in panel (B).

(B) Firing of two cells under two different odor sequences. Bars at top represent odor presentations. Bar graph represents the mitral cell odor response as defined by the first PCA component (R_j in Equation 1). This was obtained by projecting the firing pattern during the odor presentation onto the first principal component [$P_1(\phi)$ in Equation 1] plotted on the right (PC1). The response magnitude is scaled such that during an air control the average response is 0, and the standard deviation is 1 (Equation 2).

nonresponsive regions on the bulb surface were identified, and their intensity changes analyzed in the same way as for the overt spots (Figure 5A).

Following the same strategy applied to mitral cell recordings, we then identified the response of a glomerulus as significant if the intensity change exceeded a certain threshold. By varying that threshold, we followed the number of hits among glomeruli and the number of false alarms in the control regions, resulting in the ROC curve of Figure 5B. Again, we chose a threshold admitting a 10% rate of false alarms.

With this criterion for significance, one can analyze how many odors activate a glomerulus (Figure 5C). About 200 glomeruli are within view on the dorsal olfactory bulb preparation (Meister and Bonhoeffer, 2001), and ~3/4 of these were not activated by any of the 40 odors. On average, each glomerulus responded to 1.2 odors in that panel, but the histogram shows a strong tail with considerably more promiscuous glomeruli (Figure 5C).

The glomeruli activated by the odor panel were not clustered, but rather evenly distributed on the dorsal olfactory bulb (Figure 5A). The mitral cells we recorded were all situated near the middle of this field. In this light, the observation that over half of these mitral cells did not respond to any odor (Figure 4B) becomes more compelling: all of them should have had at least one strongly activated glomerulus within reach of the lateral dendrites. The next section will investigate this in more detail.

A Strong and Dense Receptive Field Is Inconsistent with Mitral Cell Responses

Whereas the previous section quantified how responsive mitral cells and glomeruli are, we now use a simple model to compare these numbers. If one assumes that the mitral cell has a dense receptive field among glomeruli (Figure 1B), then its activity should be influenced by all glomeruli within the area covered by its secondary dendrites. We did not reconstruct the dendritic trees of the recorded mitral cells, but for concreteness we will suppose that the lateral dendrites integrate information from glomeruli over an area of radius 880 μm, a typical radius for the dendritic field (Egger and Urban, 2006; Onoda and Mori, 1980). Note that this is a conservative choice, since a mitral cell can connect via intermediary granule cells to another mitral cell up to two dendritic radii away. On the other hand, a morphological analysis concluded that the density of connections is likely negligible beyond one radius (Egger and Urban, 2006).

To predict the odor responses of a mitral cell at a given location on the dorsal bulb, we centered the integration circle at that location and counted how many of the odors activate at least one glomerulus within the circle (Figure 6A). Under these assumptions, a mitral cell recorded in the middle of this olfactory bulb should produce a substantial response to ~26 of the 40 odors (Figure 6B). Averaging this analysis over glomerular recordings from six olfactory bulbs, the number of effective odors for an average mitral cell in the dorsal area should be 22 (Figure 6C). This exceeds by more than 10-fold the experimentally observed number of 2.0 odors (Figure 4B). Recall in this context that our measure of the mitral cell response is sensitive to any change in activity, not just the overtly excitatory or inhibitory responses.

In principle, this discrepancy could be reduced if one assumes a smaller integration radius around each mitral cell, so we repeated the above calculation for different radii (Figure 6C). In order to reconcile the predicted number of effective odors with the observations, the radius must be reduced to an implausibly small 150 μm. Effectively, this would allow only two to three nearest-neighbor glomeruli to contribute to the mitral cell's activity, clearly inconsistent with the reach of the lateral dendrites.

Another way to reconcile the results would be to alter the thresholds applied to mitral cell responses (Figure 4) or glomerular responses (Figure 5). By either admitting fewer glomerular responses or more mitral cell responses, one might find a relation consistent with a large integration radius for the mitral cell. We performed the entire analysis parametrically in these thresholds (Figure S1). To match the predictions from a large integration radius, one has to adopt absurd threshold values that either reject obvious responses among glomeruli (Figure S1A) or accept clear false positives among mitral cells (Figure S1C).

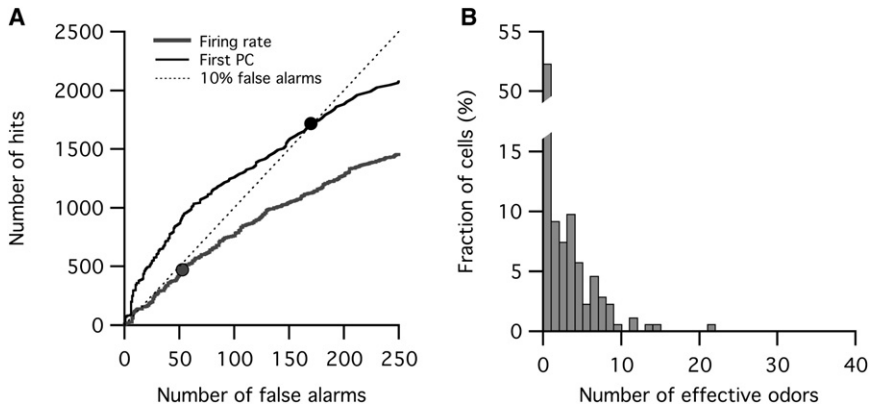

Figure 4. Sparse Odor Responses from Mitral Cells

(A) Receiver-operator characteristic of two different measures to evaluate odor responses: the firing rate and the first principal component (see Experimental Procedures). For any given threshold, we counted how many odor responses (hits) and air controls (false alarms) exceeded the threshold (among 179 cells, all odors, all repeats). While varying the threshold parametrically, the number of hits is plotted against the number of false alarms. Dotted line: ten false alarms for every 100 hits. Circles represent points on the curves closest to this 10% false alarm rate.

(B) Histogram across mitral cells of the number of odors that cause an above-threshold response, using the first principal component as a measure.

Finally one might object that the experimental response measures are imperfect. Specifically, it is possible that intrinsic signal imaging fails to detect weak responses among glomeruli. Of course, if the true response rate among glomeruli were greater, that would further increase the discrepancy here between predicted and measured results. On the side of mitral cells, we are already using very sensitive methods, recording all action potentials and analyzing them for subtle variations.

Thus, one concludes that the vast majority of glomeruli within reach of a mitral cell's secondary dendrites do not produce any noticeable response when activated individually. We will consider two ways of explaining this result. First, it is possible that the mitral cell has a dense but very weak receptive field surround. In that case, the influence of any single glomerulus, other than the principal one, may remain below the threshold of what is recognized as an odor response. Alternatively, the receptive field may be composed of the principal and just a few other glomeruli, each with a strong influence on the mitral cell response.

A Sparse Receptive Field Can Explain Mitral Cell Responses

Both the hypotheses mentioned above call for a model that allows for subthreshold summation of more subtle glomerular influences. Thus, instead of using the binary categorization into responses above or below threshold, we searched for a model that would quantitatively match the magnitude of activity in mitral cells. The simplest form of such a model involves linear summation: each mitral cell pools inputs from a set of glomeruli, and the

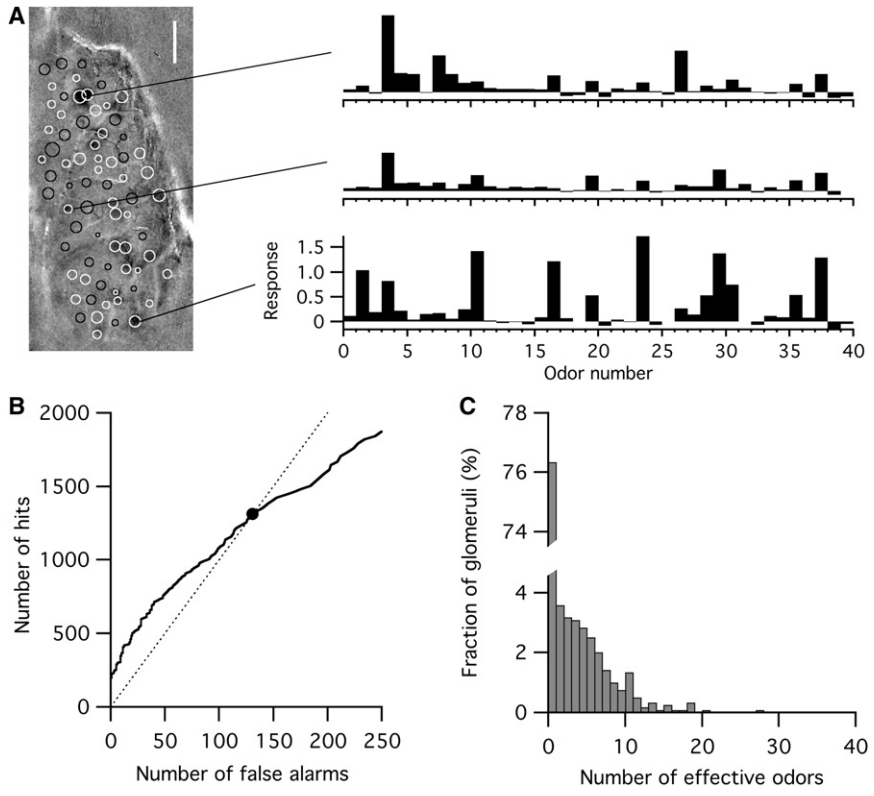

Figure 5. Sparse Odor Responses from Glomeruli

(A) (Left) Ratio image of a single odor response (ethyl butyrate) in a sample olfactory bulb. The gray scale spans a reflectance change of 0.001. Distinct spots that appeared in this or other odor images were identified as glomeruli. The white circles represent the average 1 SD radius of the two-dimensional Gaussian used to fit the spots (see Experimental Procedures). Areas without spots were used as controls to assess noise (black circles). (Right) Odor response spectra for three of the glomeruli identified in the left panel. For odor identities, see Table S2, List A. Scale bar, 500 μm.

(B) Receiver-operator characteristic of the glomerular signals. By applying a varying threshold to the signals, we counted how many glomerular regions (hits) and control regions (false alarms) exceeded the threshold (130 glomeruli, 100 odors). The number of hits is plotted against the number of false alarms. Dotted line: ten false alarms for every 100 hits. Circle identifies the threshold value yielding a 10% false alarm rate.

(C) Histogram across glomeruli of the number of odors that cause an above-threshold response, averaged over six bulbs.

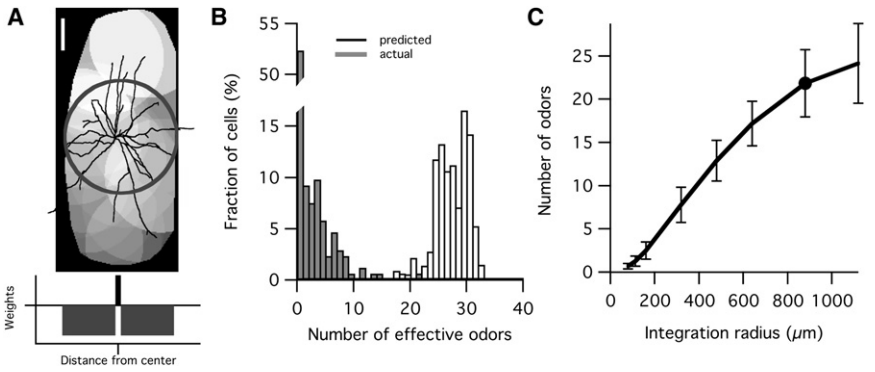

Figure 6. A Strong and Dense Receptive Field Grossly Overpredicts Mitral Cell Responses

(A) Counting the number of odors that activate glomeruli inside a mitral cell's dendritic field. Tracing illustrates the extent of a mitral cell dendritic field (from Orona et al., 1984; reprinted with permission of Wiley-Liss, Inc., a subsidiary of John Wiley & Sons, Inc). The circle indicates the integration radius of 880 μm assumed for the present calculation. For each location on the dorsal olfactory bulb, we counted how many odors activate at least one glomerulus less than one integration radius away. The resulting number is encoded in grayscale (black = 0, white = 32). Scale bar, 500 μm. Lower diagram: icon representing the shape of this receptive field model, with a strong contribution from glomeruli anywhere inside a defined radius.

(B) Histogram of the number of odors predicted to activate a mitral cell near the middle of the dorsal bulb in panel (A), where the recording electrodes were placed. For comparison, the graph reproduces the actual observed histogram (from Figure 4B).

(C) We varied the radius of the integration circle (panel [A]) and repeated the analysis of panel (B). Shown here is the predicted number of effective odors as a function of the integration radius (average ± SD across six olfactory bulbs). Filled circle indicates the radius used in panels (A) and (B).

signal in each glomerulus is weighted by a factor representing its "connection strength" (Equation 3). One can now compare different hypotheses for these weighting factors.

To implement a dense but weak surround, we gave the cell's primary glomerulus a strong weight and all other glomeruli a small weight, decreasing with distance from the primary glomerulus. The primary glomerulus was taken to be the one whose odor-response spectrum was most highly correlated with that of the mitral cell. The weights of the surrounding glomeruli declined as a Gaussian function of distance (Equation 5 and Figure 7A). In fitting this receptive field, we adjusted the strength of the contributions of the primary glomerulus and the surround to minimize the difference between the simulated and the observed odor responses (see Experimental Procedures). In general, the resulting fit quality was quite poor. One of the best examples is displayed in Figure 7: note that there is significant discrepancy between the predicted and measured odor-response spectrum (Figure 7B). Furthermore, the surround in this fit makes very little contribution to the response (Figure 7C).

To implement a sparse receptive field, we assumed that just a few glomeruli made strong contributions (Figure 8A). Given the earlier observation that only a handful of glomeruli are needed to explain the frequency of mitral cell responses (Figure 6C), we allowed for four glomeruli in this receptive field model. However, unlike in Figure 6C, these glomeruli were not restricted to adjacent locations. For any given mitral cell, the identities and weights of those glomeruli were optimized. The fits obtained with this sparse model were markedly better (Figure 8B). For many mitral cells, the residual of the fit was comparable to the trial-to-trial noise in the response (Figure 8B). This means that the model can predict mitral cell responses from glomerular activity with the same accuracy at which the brain produces them. For some mitral cells with low noise, we encountered interesting discrepancies, where the response to certain

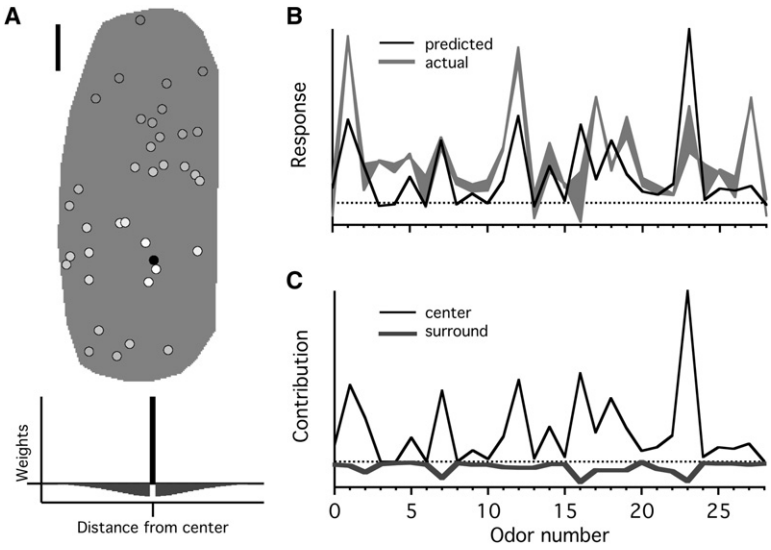

Figure 7. A Weak and Dense Receptive Field Does Not Explain the Odor Spectra of Mitral Cells

(A) A sample receptive field fit to predict a mitral cell response using the Gaussian surround model. Outline of the olfactory bulb with the optimized weights of different glomeruli shown on a gray scale (black: center glomerulus with positive weight, white: negative weight, gray: zero weight). Scale bar, 500 μm. Lower diagram: icon representing the shape of this receptive field model, with a graded contribution from surround glomeruli declining with distance from the center.

(B) The odor response spectrum of the mitral cell predicted from this receptive field, compared to the actual response in two stimulus repeats. For odor identities see Table S2, List C.

(C) The contributions to the spectrum in panel (B) from the center glomerulus and all the surround glomeruli.

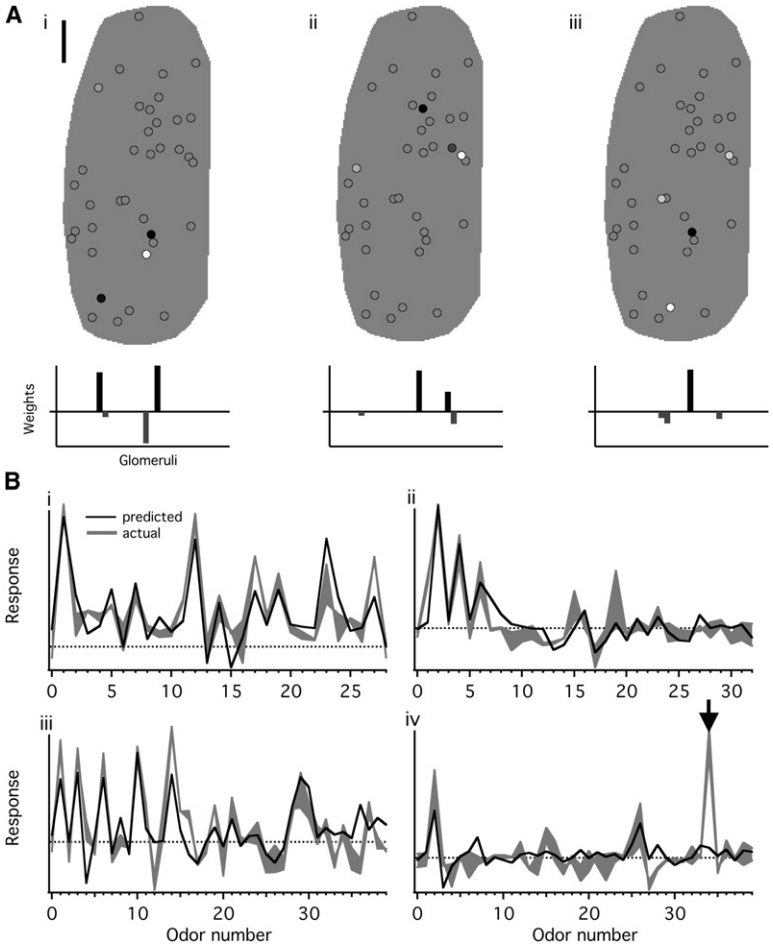

Figure 8. A Sparse Receptive Field Can Explain the Odor Spectra of Mitral Cells

(Ai) A sample fit to predict a mitral cell response using a sparse receptive field with just four glomeruli, displayed as in Figure 7A. In this case, two of the glomeruli have positive weights, and two negative. Note that this need not represent net excitatory and inhibitory effects, but they do affect the phase distribution of spikes in opposite ways. Lower diagram: icon representing the shape of this receptive field model with contributions from a discrete set of glomeruli. Scale bar, 500 μm. (Aii and Aiii) Examples of fits for two other mitral cells, displayed as in (Ai).

(Bi) Odor response spectrum predicted by the receptive field in panel (Ai), compared to the actual response of this mitral cell (same neuron as in Figure 7, display as in Figure 7B). (Bii and Biii) Odor response spectra and their fits for the mitral cells in panels (Aii) and (Aiii). (Biv) Odor response spectrum and its fit for another mitral cell. Arrowhead indicates a clear omission in the predicted spectrum; presumably, the glomerulus mediating this response lies outside the window of observation. For odor identities see Table S2, List A (Biii and Biv), List B (Bii), and List C (Bi).

odors could not be fitted at all (Figure 8B). In those cases, the odor in question did not activate any glomerulus that we recorded; presumably, the glomerulus that caused the mitral cell response was outside the dorsal window of view. Note that such discrete failures are a hallmark of the sparse receptive field model, and not expected under a dense receptive field hypothesis.

To summarize results from this analysis over many mitral cells, we compared the goodness of fit for the different receptive field models (Figure 9A). To enhance confidence in the results, this analysis was restricted only to mitral cells with the most reproducible responses (see Experimental Procedures). We found that the sparse receptive field performed significantly better than either a dense receptive field or a field consisting of a single glomerulus (Figure 9A).

Note that the sparse receptive field model (Figure 8A) has a few more degrees of freedom than the dense receptive field (Figure 7A). One might be concerned that these additional parameters allow for "overfitting" of the response data, namely an improvement of the fit quality without extracting any underlying structure in the data. To explore this, we performed a shuffle test: the measured odor-response spectrum of each glomerulus was shuffled randomly, and the analysis was repeated. The resulting sparse fits were poor, comparable to the dense and single-glomerular fits (Figure 9A). We conclude that the sparse receptive field model does not suffer from overfitting and truly represents a superior description of the interactions between glomeruli and mitral cells.

Given that a mitral cell is only influenced by a few glomeruli, we asked whether these glomeruli have any distinguishing features in common. First, we considered their spatial proximity on the olfactory bulb. It emerged that the glomeruli used to compose a mitral cell's receptive field are no closer together than any randomly selected glomeruli within the dorsal observation window (Figure 9B). Then, we inspected their odor-response spectra and analyzed their degree of overlap (see Experimental Procedures). By this criterion as well, the glomeruli contributing to a mitral cell response are no more similar than any glomeruli picked by chance (Figure 9C).

DISCUSSION

In this study, we investigated the functional connectivity patterns between inputs and outputs of the olfactory bulb. Specifically, we tested the relationship between signals in glomeruli and the responses of mitral cells. It has been suggested that a mitral cell gets excited by a single central glomerulus and receives broad and predominantly inhibitory inputs from a large surrounding field of glomeruli. We found that this dense receptive field model is inconsistent with the observed odor responses (Figures 6, 7, and 9). Instead, a small number of glomeruli seem to contribute strongly to the mitral cell's activity and can account for most of its odor response (Figures 8 and 9). Furthermore, the glomeruli that constitute this sparse receptive field tend to be chemically dissimilar and spatially dispersed on the bulb (Figure 9). This represents a fundamental revision of the nature of signal flow in the olfactory bulb. We discuss briefly the basis for these

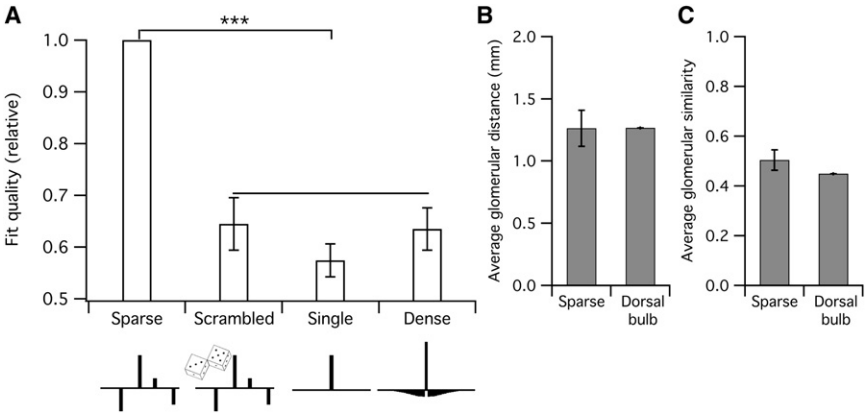

Figure 9. Statistics of Sparse Receptive Field Models and Their Constituting Glomeruli

(A) The fit quality (see Experimental Procedures) for different receptive field models applied to the same mitral cell response. Sparse: sparse receptive field fit with four glomeruli. Scrambled: sparse receptive field fit applied to scrambled glomerular odor spectra, as a control for overfitting. Single: best fit using a single glomerulus. Dense: a center glomerulus with Gaussian surround. The fit quality is expressed relative to that for the sparse receptive field and averaged over 11 cells with high signal-to-noise ratio (mean ± SEM). The difference marked *** is significant at $p < 0.001$.

(B) Physical distance between glomeruli contributing to a mitral cell. For the four glomeruli in a mitral cell's sparse receptive field, we computed the average pairwise distance. This was compared to the average pairwise distance of any two glomeruli in the window of observation on the dorsal bulb. Results from 11 cells with high signal-to-noise ratio, mean ± SEM.

(C) Chemical similarity among glomeruli contributing to a mitral cell. For the four glomeruli contributing to a mitral cell's sparse receptive field, we computed the average pairwise overlap of their odor response spectra (see Experimental Procedures). This was compared to the average overlap for any two glomeruli in the dorsal bulb. Results from 11 cells with high signal-to-noise ratio, mean ± SEM.

conclusions and their implications for the nature of odor processing.

Sparse Odor Responses from Mitral Cells

Individual mitral cells responded to very few odors in our panel (Figure 4): about 50% gave no response, and the other neurons detected a median of 3 of the 40 odors. Although it is difficult to compare such percentages across studies, the sparse odor sensitivities observed here are similar to other recordings from mitral cells at low odor concentrations (Davison and Katz, 2007; Lin et al., 2005). The surprise in the present study came from a comparison to odor responses in glomeruli under the same stimuli. In the vicinity of any mitral cell, there were in fact many glomeruli activated by the odor panel, but most of them did not influence the cell's firing. Under the conventional hypothesis of a dense receptive field for mitral cells, one would have predicted a far broader odor-response spectrum than observed (Figure 6). Even though the general mitral cell behavior we observed is in line with prior studies, it is worth discussing some methodological concerns and how they might affect the conclusions in favor of a sparse receptive field.

Extracellular recordings are invariably biased in favor of neurons that fire and respond to the stimulus. Thus, we may have missed a number of mitral cells that remained silent for all the odors tested, and therefore the stated fraction of responsive mitral cells is an upper bound. For the cells we did record, we recorded every action potential and tried hard to sensitively detect any change in the firing pattern (Figures 2 and 3). By comparison, the intrinsic imaging method observes all the glomeruli on the dorsal olfactory bulb. This technique has its own limitations; for example, it cannot resolve rapid modulations in firing (Spors and Grinvald, 2002). Thus, we may well have missed some odor responses in receptors that can influence mitral cell firing, and therefore the reported fraction of responsive glomeruli is a lower bound. All of these biases work in the same direction: they strengthen the conclusion in favor of a sparse receptive field.

Another potential concern relates to anesthesia, specifically whether this can account for the sparseness of odor responses in mitral cells. As in many studies of olfactory bulb physiology, we used urethane because it has more subtle effects on neural activity than barbiturates or ketamine (Hara and Harris, 2002; Neville and Haberly, 2003). Still, activity in the olfactory bulb differs greatly between the awake and the anesthetized state (Rinberg and Gelperin, 2006). Perhaps the most dramatic difference is that odor responses are clear and distinct under anesthesia, whereas they are often hard to detect in the awake state (Adrian, 1950; Kay and Laurent, 1999; Rinberg et al., 2006). Thus, the use of anesthesia should bias the fraction of responsive mitral cells upward, which again strengthens the evidence in favor of a sparse receptive field.

Sparse Connections between Glomeruli and Mitral Cells

Going beyond the statistics of response frequencies among glomeruli and mitral cells, we searched for a deterministic and quantitative relationship that would predict the response of a given mitral cell from the activation of the overlying glomeruli. We found that simple linear summation of glomerular inputs provided a successful fit of many mitral cell response spectra (Figures 8 and 9). By inspecting the weights applied to individual glomeruli in this model, it emerged that just a few glomeruli make strong contributions to any given mitral cell. Generally, there was not a single dominant glomerulus, but several with comparable contributions (Figures 8A and 9A) distributed sparsely over some distance (Figure 9B). Furthermore, these major glomeruli often had effects of the same sign, indicating that they affect the phase distribution of mitral cell spikes in the same direction (Figure 8A). None of these aspects is reflected in the center-surround model for the mitral cell receptive field, in which a central glomerulus is surrounded by a broad antagonistic region. Indeed, this dense receptive field model was clearly inconsistent with the measurements (Figures 7 and 9). Several recent studies touch directly on this conclusion.

The experiments by Luo and Katz (2001) are conceptually closely related and appear to lead to a different result, namely

a receptive field with a dense antagonistic surround. These authors recorded odor responses intracellularly from mouse mitral cells, along with the response patterns of glomeruli. Between four and six odors were used at high concentration to increase the probability of mitral cell responses. More importantly, a different method was applied in computing the receptive field of the mitral cell. Whenever an odor elicited a measurable response, the procedure added that odor's glomerular activation pattern as a contribution to the receptive field. Recall that each odor typically activates several glomeruli. If only one of those caused the mitral cell response, then the other glomeruli were added to the receptive field inappropriately; examples of this occur in the published data (e.g., Figure 1A, panels 4–5 of Luo and Katz, 2001). Clearly, this method—technically called a reverse correlation—overestimates the receptive field, because of the correlations in the glomerular response patterns. By comparison, the method applied here—technically a least-squares regression—corrects for these correlations and isolates those glomeruli that actually have a functional contribution to the mitral cell (Willmore and Smyth, 2003). This approach requires a large number of odors applied at low concentration, since that increases the number of independent observations that constrain the weight of any given glomerulus. On balance therefore, the report of Luo and Katz (2001) remains compatible with a sparse receptive field.

Another study came to a conclusion at the opposite extreme, namely that each mitral cell is controlled exclusively by a single glomerulus (Arenkiel et al., 2007). Here, the glomeruli were activated not by odors but by spots of light, using a transgenic mouse expressing channelrhodopsin-2 in mitral cells. A small spot centered on the recorded mitral cell produced clear excitation, but additional spots of light anywhere on the olfactory bulb had no effect on the firing rate. This is difficult to reconcile with the present results (Figure 9A) or indeed with any number of studies documenting lateral interactions among glomeruli (Egger and Urban, 2006; Wachowiak and Shipley, 2006). Among other things, it is difficult to understand why a mitral cell should be inhibited by some odors and excited by others (e.g., Figure 2). Perhaps the lateral integration of signals is contingent on the periodic modulation of mitral cell spikes by the inhalations, which is provided by odor stimulation but not by light activation. Similarly, some mitral cell responses do not involve an overt change in average firing rate (Figure 2). Given the obvious power of the light stimulation approach, this will undoubtedly be explored further.

A recent anatomical study investigated lateral connectivity using a retrograde tracer that spreads across synapses (Willhite et al., 2006). A modified pseudorabies virus was injected either at a discrete location in the olfactory bulb or into one of its target areas, and the spread of virus within the bulb was assessed at various times after infection. If the lateral connections of a mitral cell were dense and continuous in space, one would expect a broad and uniform lateral spread of infection. Instead, the virus labeled a few discrete columns of the bulb. Each column typically ran from the granule cell layer to the glomerular layer and often encompassed just an individual isolated glomerulus. The authors suggest that individual mitral cells have anatomical connections to just a sparse subset of surrounding glomeruli, consistent with the conclusions from the present physiological study.

Finally, there is circumstantial evidence favoring this view. Under the hypothesis of a dense inhibitory surround, all of the 25–50 mitral cells with the same principal glomerulus should share approximately the same inhibitory inputs. By contrast, a sparse lateral connectivity would allow each of those neurons to establish different lateral connections. Prior work indeed suggests that mitral cells with the same principal glomerulus can have quite different odor-response spectra (Motokizawa, 1996; Egana et al., 2005). An earlier study of nearby mitral cells (Buonviso and Chaput, 1990) had placed more emphasis on the similarity of their odor responses. However, this similarity was limited to shared excitation, whereas the inhibitory responses were as different in nearby cells as in distant cells. Thus, all of these reports imply that mitral cells with the same principal glomerulus can have substantially different inhibitory input, which speaks in favor of sparse lateral connectivity.

Implications for Olfactory Processing

Given the circuitry in the olfactory bulb, it has been postulated that the role of lateral inhibition is to reduce correlations in the olfactory signal presented to the animal (Mori and Shepherd, 1994; Yokoi et al., 1995). Specifically, it might sharpen a mitral cell's receptive range for odor stimuli, in the same way as visual receptive fields are sharpened in the retina. To sustain this analogy, one must assume that the olfactory receptors are sensitive to a broad range of odors and that this receptive range varies smoothly with position on the glomerular layer. Furthermore, one supposes that each mitral cell has a dense inhibitory field surrounding it. In this way, the receptive range of its principal glomerulus can be trimmed by subtracting the overlapping receptive ranges of neighboring glomeruli to produce a sharper odor sensitivity (Yokoi et al., 1995).

However, this analogy suffers on two levels. First, there is no smooth chemotopic mapping of the molecular receptive range onto the olfactory bulb surface. Unlike the case of the retina, where a point of light produces a dense focus of activity in the neural sheet, a discrete odor produces a dispersed pattern of active glomeruli (Meister and Bonhoeffer, 2001; Rubin and Katz, 1999; Uchida et al., 2000). While certain classes of odors preferentially activate one domain of the bulb (Mori et al., 2006; Johnson and Leon, 2007), that domain also contains glomeruli that respond to entirely different odor classes (Friedrich and Korsching, 1997; Meister and Bonhoeffer, 2001; E.R.S. et al., unpublished data). Thus, each mitral cell finds in its vicinity glomeruli with a great diversity of odor spectra. Second, it appears from the current and other studies discussed above that the lateral interactions may well be sparse rather than diffuse as in the retina.

Thus, one is led to a different view of computation by mitral cells: each mitral cell has within reach of its lateral dendrites glomeruli with a broad diversity of odor sensitivities, whose outputs could be compared to that of its principal glomerulus. Depending on the olfactory tasks, any number of these comparisons might be computationally useful. This leads one to revisit the original proposal for sharpening a mitral cell's receptive range. In principle, the sparse pattern of connections could be used for

precisely that purpose: a mitral cell might "select" within the diverse field of surrounding glomeruli those whose odor spectra have partial overlap with that of the principal glomerulus and thus sharpen its odor sensitivity. However, we found no evidence for such a principle: the glomeruli that contributed to the same mitral cell showed no special relationship between their odor spectra (Figure 9C).

What the actual rules are by which odor sensitivities are combined at mitral cells will be of continuing future interest. As discussed above, this question bears great potential richness, since each of the many mitral cells in one glomerulus may perform a different comparison. Which of these are actually implemented is determined by the mitral/granule cell synapses in the dendritic field. The state of those synapses is likely under flexible control: on a moment-to-moment basis, the lateral influence may change depending on neural activity in the mitral cell itself (Arevian et al., 2008). Centrifugal signals may modulate the state of the connections on a longer timescale (McLean and Shipley, 1991), and it may be influenced by recent experience, for example to implement storage and recall of odor patterns (Brennan and Keverne, 1997).

EXPERIMENTAL PROCEDURES

Subjects

The experiments were performed in the rat. Although the mouse is increasingly gaining popularity as a research subject, the following criteria motivated this choice. First, the glomeruli in the rat olfactory bulb are more easily resolved in imaging experiments, owing to their larger size, and this provides a better estimate of their odor activation spectrum. Also, in our experience, rats allow for longer and more stable experiments than mice. The present studies required stimulation with a large panel of odors and multiple replicate repeats. Extracellular recordings of mitral cells lasted for up to 24 hr, and imaging experiments up to 40 hr. Finally, most of the prior work on neurophysiology in the bulb has been performed in the rat, and it was essential to link to this literature. In any case, the indications to date are that neuronal circuitry is rather similar across mammalian olfactory bulbs.

A total of 54 adult rats (female Wistar, ~300 g) contributed to the experiments reported here. The animal was anesthetized with urethane (12.5% IP, initial dose 2–4 ml, to a level of 1.5 g/kg) and atropine (25 μg/kg IP) and mounted in a stereotaxic frame. In order to prevent fluid collection in the nasal cavity, 4 mg/kg diphenhydramine (Benadryl) was injected in the leg muscle. Heartbeat, respiratory rate, and lack of pain reflexes were monitored throughout the experiment. If needed, more urethane was injected, in 0.5 ml steps. Before starting the surgery, a local anesthetic was injected under the skin on top of the skull. The animal was placed on a heat pad, held at 37°C, monitored with a rectal probe. As the experiments lasted many hours, sterile 0.9% saline solution was injected periodically under the skin in the back of the rat. No respirator was used, and the animal breathed freely through the nose, at a rate of 1.5–2.5 inspirations/s.

All animal procedures conformed to NIH guidelines and were approved by Harvard University's Animal Care and Use Committee.

Stimulus Presentation

A machine was designed to rapidly deliver 100 different odors in arbitrary sequence. Odorants were diluted in mineral oil (1:100, typically), absorbed onto filter paper, and stored in glass vials sealed with a thick rubber septum (Vacutainer #366431 tubes). Under computer control, the desired tube was positioned under a pair of 20 gauge noncoring needles (Popper and Sons, Inc. #7184) using two linear translators, and a third translator pushed the needle assembly through the septum. Clean, filtered, and humidified air entered through one needle, and the odor stream exited through the other needle at a rate of 1 l/min. Teflon-coated tubing carried the stimulus to the rat via an anesthesia mask surrounding the animal's snout.

For several odorants representing different chemical classes, we measured the concentration in the vapor delivered to the animal, using a flame ionization detector (FID). Typically, the odors delivered to the rat were in the concentration range of 0.1%–1% of the saturated vapor at room temperature. These concentrations are low enough to avoid saturation of receptors (Meister and Bonhoeffer, 2001). A total of ~200 odors were tested, and among these a set of 40 was used most frequently, chosen for their ability to activate glomeruli and mitral cells on the dorsal side of the olfactory bulb (Table S2, List A). Occasionally, a different set of odors was used. A list of all odors and the specific sets used in each figure are provided in Table S2.

Intrinsic Imaging

For imaging experiments, the skull was thinned with a dental drill to reveal the olfactory bulbs underneath or was completely removed, leaving the dura intact. Low melting point agarose (1.5%) was poured over the opening and topped with a clear coverslip. To prevent the drying of the agarose and formation of air bubbles, a ring of Vaseline was applied at the interface of glass and agarose.

The dorsal side of the olfactory bulb was illuminated with 700 nm red light, produced by filtering light from a stable incandescent lamp. The images were recorded at a resolution of 16 μm/pixel and 24 frames/s using a digital camera (Vosskuehler CCD-1300F) combined with a digital frame-grabber card (PCI-1322, National Instruments) and custom-written software in Labview. Acquisition began 10 s prior to odor delivery and continued for 30 s during odor presentation. The time-averaged image during stimulation was divided by the time-averaged image prior to stimulation. These ratio images were further averaged over 8 to 15 trials with the same odor, interleaved with other odor trials. To suppress contamination from a large-scale hemodynamic signal (Meister and Bonhoeffer, 2001), the ratio image was spatially high-pass filtered by subtracting a copy that was convolved with a Gaussian spatial kernel with a standard deviation of 330 μm.

Electrophysiology

For electrical recordings, the bone overlying the middle of the dorsal olfactory bulbs was completely removed, leaving the dura intact. After insertion of the electrodes, all exposed brain areas were covered with low melting point agarose (3%) in order to prevent the drying of tissue and reduce vibration. Finally, Vaseline or mineral oil were applied to the top of the agarose layer to prevent it from drying out.

Recordings were performed with pulled-glass pipettes, filled with 2 M NaCl, of 0.5–3 MOhm impedance, tungsten electrodes (A-M Systems #5753, 5 MOhm), or tetrodes (NeuroNexus Technologies, 16 channel tetrodes, 300–500 kOhm impedance). For stimulation of the lateral olfactory tract (LOT), a concentric tungsten electrode (WPI, #TM33CCNON) was inserted stereotaxically into the forebrain, at 2.7 mm anterior from the bregma, 3.2 mm lateral from the midline, and 6 mm deep from the surface, or until neuronal firing was encountered phaselocked to the respiration (Nagayama et al., 2004). Electrodes were positioned with a Sutter Instruments MP-285 micromanipulator. Extracellular recordings were processed with an A-M Systems 1800 amplifier, or a custom-built amplifier, filtered at 300 Hz to 2 kHz.

The antidromic LOT stimuli were delivered using an A-M Systems 2100 stimulator (1–10 V, 10 μs, monophasic or biphasic). This served to guide placement of the recording electrode, which was advanced to the level where the field potential from LOT stimulation reversed (Rall and Shepherd, 1968). For some units, we confirmed the presence of an axon in the LOT by spike collision tests (Scott, 1981). Based on the location of the recording electrode, the units were likely not external tufted cells. Beyond that, we could not distinguish mitral from tufted cells. We will call the recorded neurons "mitral cells" for short.

The respiration events were recorded using a piezoelectric sensor placed under the animal at the level of the diaphragm. Phase 0 of each respiratory cycle corresponds to the beginning of inhalation. However, in some experiments the probe was inadvertently placed at a different location, and the absolute

phase values may differ slightly. This is of no consequence to the analysis presented.

Owing to the long duration of the required stimulus sequences, we generally performed the imaging and recording experiments in different animals. The odor spectra and spatial locations of glomeruli are well conserved across individuals (Strotmann et al., 2000; Wachowiak and Cohen, 2001). In recent work, we measured the variability in the position of glomeruli on the rat dorsal bulb: ±1 positions (RMS scatter) mediolateral and ±2 positions anteroposterior (E.R.S. et al., unpublished data). Thus, comparing a mitral cell in one animal with glomeruli in another animal introduces only a small uncertainty about the location of specific glomeruli. This does not affect the basic distinction between dense and sparse receptive fields. Similarly, the uncertainty is much smaller than the typical distance we found between glomeruli that contribute to a mitral cell (Figure 9B).

Analysis

Glomerular Response

The ratio images of the olfactory bulb surface often showed small (80–200 μm diameter) round spots (Figure 5), which were taken to reflect activity in individual glomeruli, based on previous work (Meister and Bonhoeffer, 2001). Each spot was fitted with a two-dimensional Gaussian, and the response strength G_{ij} of glomerulus i to odor j is reported as the amplitude of the Gaussian in that odor's intrinsic image. For the purpose of ROC analysis (Figure 5), some areas of the image with no overt spots were treated in the same way to produce a set of controls. Many glomeruli responded to none of the odors tested, and that fraction was estimated using the fact that ~200 glomeruli lie within view of the dorsal craniotomy (Meister and Bonhoeffer, 2001).

Spike Sorting

Action potentials in the extracellular recording were identified by standard manual clustering methods. In short, the raw electrical recording was digitized at 10 kSamples/s. A threshold was selected above the noise level, and spike waveforms were cut from 0.3 ms before to 1.2 ms after the positive threshold crossing. A PCA was performed on the collection of all these waveforms, and the data were projected onto the first two principal components. In this two-dimensional shape space, clearly distinct clusters were selected manually, and the collection of arrival times of the events in the cluster was defined as one spike train. Using an interspike interval plot, we required a refractory period of >2 ms before accepting a spike train as a "single unit."

Phase Plots

To compactly display the dynamics of a mitral cell's odor response (Figures 2, 3, and S1), we employed 2-dimensional phase plots (Macrides and Chorover, 1972). Each vertical column corresponds to one respiration cycle, with phase ranging from $\phi = 0$ to $\phi = 2\pi$. Within that column, the spike times are histogrammed in ten bins of phase, and the result shown on a gray scale. Finer phase binning did not improve the analysis of firing patterns.

Principal Component Analysis

For each cell, and every odor stimulus j, we computed the phase histogram of spike times averaged over the interval of odor presentation, $r_j^{(O)}(\phi)$, during the first half of the preceding air presentation, $r_j^{(A1)}(\phi)$, and during the second half of the air presentation, $r_j^{(A2)}(\phi)$. We defined the response to odor j as $R_j(\phi) = r_j^{(O)}(\phi) - r_j^{(A1)}(\phi)$, and the corresponding air control as $C_j(\phi) = r_j^{(A2)}(\phi) - r_j^{(A1)}(\phi)$. A PCA was then performed on the collection of all the firing patterns $R_j(\phi)$ and $C_j(\phi)$. The resulting eigenvectors were used as basis vectors on which the firing patterns were projected (Figure 3). In practice, the first eigenvector, $P_1(\phi)$, accounted for a good fraction of the variance in the data set; there was a large decline in the variance from the first to the second component and a gradual decline for higher components (Figure 3A). As always, some of the variance in the data set results from uncontrolled variables of the experiment (usually called "noise"), and it is beneficial to remove these components before further analysis. We obtained a conservative estimate of the noise variance by a shuffle test: the matrix elements of the phase plot (e.g., Figure 2E) were reordered randomly, and the PCA procedure was repeated (Figure 3A). Only the first principal component of the data was found to have variance substantially above the level expected from noise.

For further analysis, we quantified the firing patterns during odor or air controls by the projection on the first eigenvector:

$$\begin{aligned} R_j &= a + b \int_0^{2\pi} R_j(\phi) \cdot P_1(\phi) d\phi \\ C_j &= a + b \int_0^{2\pi} C_j(\phi) \cdot P_1(\phi) d\phi \end{aligned} \quad (1)$$

where the scaling factors a and b were chosen such that the air controls are normalized to zero mean and unit standard deviation,

$$\langle C_j \rangle = 0 \text{ and } \left\langle C_j^2 \right\rangle - \langle C_j \rangle^2 = 1. \quad (2)$$

At later stages of the analysis, we verified again that projection onto a single principal component is sufficient. For example, we performed the ROC analysis of Figure 4 including the second and higher components. The ROC curve did not improve significantly beyond what was obtained with the first principal component.

Linear Fits

We used a linear approximation of the relationship between glomerular and mitral cell responses, in which the predicted mitral cell response R_j' to odor j is given by:

$$R_j' = \sum_{i=1}^{m} G_{ij} \cdot w_i \quad (3)$$

where G_{ij} is the response of the glomerulus i to odor j, w_i is the influence of glomerulus i on the mitral cell response, and m is the total number of glomeruli used. In order to optimize the fit, we compared the actual mitral cell responses R_j to the predicted responses R_j', and found the weighting factors w_i that minimized the squared error over all n odors:

$$E = \sum_{j=1}^{n} \left(R_j - R_j' \right)^2. \quad (4)$$

This optimization was subject to constraints, depending on the specific receptive field model.

Center-Surround Fits

In the receptive field model with a dense antagonistic surround (Figure 7), we assumed that a single center glomerulus made a strong contribution to the response, and the strength of other glomeruli declined as a monotonic function of distance from the center, specifically:

$$\begin{aligned} w_c &= A \\ w_{i \neq c} &= B \cdot e^{-d_{ic}^2 / 2L^2} \end{aligned} \quad (5)$$

where d_{ic} is the distance between glomeruli i and c, and L is the dendritic integration radius. The center glomerulus c was chosen as the one whose odor responses G_{cj} had the highest correlation coefficient with the mitral cell responses, R_j. The parameters A and B represent the strength of the center and the surround respectively, and their values were chosen to minimize E (Equation 4).

Sparse Fits

In the sparse receptive field model (Figure 8), we assumed that only four glomeruli contribute to the response,

$$w_i = 0, \text{ if } i \notin \{a, b, c, d\}. \quad (6)$$

The identities $\{a, b, c, d\}$ of the four glomeruli and their associated weights $\{w_a, w_b, w_c, w_d\}$ were chosen to minimize E (Equation 4) by numerical search.

Goodness of Fit

In comparing the various receptive field models, we limited analysis to a set of mitral cells with high signal-to-noise ratio. The signal was assessed by the power in the response across odors,

$$S = \sum_{j=1}^{n} R_j^2. \quad (7)$$

The noise was assessed by the squared deviation of the response across two repeats of the same odor sequence,

$$N = \sum_{j=1}^{n} \left(R_j^{(1)} - R_j^{(2)} \right)^2. \quad (8)$$

By this measure of S/N we selected the best 10% of cells for which at least two stimulus repeats were recorded.

The goodness of fit of each model was then evaluated by comparing the error of the model prediction (Equation 4) to the signal power in the response (Equation 7),

$$F = 1 - \frac{E}{S} = 1 - \frac{\sum_{j=1}^{N} \left(R_j' - R_j \right)^2}{\sum_{j=1}^{M} R_j^2}. \quad (9)$$

This reflects the fraction of the power in the response that is captured by the model.

Similarity of Glomeruli

We measured the chemical similarity O_{ab} of two glomeruli a and b by the overlap of their odor response spectra, specifically the uncentered correlation coefficient

$$O_{ab} = \frac{\sum_{j=1}^{n} G_{aj} G_{bj}}{\sqrt{\sum_{j=1}^{n} G_{aj}^2} \cdot \sqrt{\sum_{j=1}^{n} G_{bj}^2}}. \quad (10)$$

Glomeruli with the same odor response spectrum will have a similarity of 1, while glomeruli that respond to perfectly nonoverlapping odor sets have a similarity of 0. To assess the chemical similarity among a set of four glomeruli (Figure 9C), we averaged all the pairwise similarities of the glomeruli within the group.

SUPPLEMENTAL DATA

The Supplemental Data include figures and tables and can be found with this article online at http://www.neuron.org/cgi/content/full/59/5/802/DC1/.

ACKNOWLEDGMENTS

We thank Catherine Dulac, John Kauer, Venki Murthy, Clay Reid, Carla Shatz, Rachel Wilson, and members of the Meister lab for support and many helpful discussions.

Accepted: July 28, 2008
Published: September 10, 2008

REFERENCES

Adrian, E.D. (1942). Olfactory reactions in the brain of the hedgehog. J. Physiol. *100*, 459–473.

Adrian, E.D. (1950). The electrical activity of the mammalian olfactory bulb. Electroencephalogr. Clin. Neurophysiol. *2*, 377–388.

Arenkiel, B.R., Peca, J., Davison, I.G., Feliciano, C., Deisseroth, K., Augustine, G.J., Ehlers, M.D., and Feng, G. (2007). In vivo light-induced activation of neural circuitry in transgenic mice expressing channelrhodopsin-2. Neuron *54*, 205–218.

Arevian, A.C., Kapoor, V., and Urban, N.N. (2008). Activity-dependent gating of lateral inhibition in the mouse olfactory bulb. Nat. Neurosci. *11*, 80–87.

Aungst, J.L., Heyward, P.M., Puche, A.C., Karnup, S.V., Hayar, A., Szabo, G., and Shipley, M.T. (2003). Centre-surround inhibition among olfactory bulb glomeruli. Nature *426*, 623–629.

Brennan, P.A., and Keverne, E.B. (1997). Neural mechanisms of mammalian olfactory learning. Prog. Neurobiol. *51*, 457–481.

Buonviso, N., and Chaput, M.A. (1990). Response similarity to odors in olfactory bulb output cells presumed to be connected to the same glomerulus: electrophysiological study using simultaneous single-unit recordings. J. Neurophysiol. *63*, 447–454.

Chaput, M.A., Buonviso, N., and Berthommier, F. (1992). Temporal patterns in spontaneous and odour-evoked mitral cell discharges recorded in anaesthetized freely breathing animals. Eur. J. Neurosci. *4*, 813–822.

Davison, I.G., and Katz, L.C. (2007). Sparse and selective odor coding by mitral/tufted neurons in the main olfactory bulb. J. Neurosci. *27*, 2091–2101.

Egana, J.I., Aylwin, M.L., and Maldonado, P.E. (2005). Odor response properties of neighboring mitral/tufted cells in the rat olfactory bulb. Neuroscience *134*, 1069–1080.

Egger, V., and Urban, N.N. (2006). Dynamic connectivity in the mitral cell-granule cell microcircuit. Semin. Cell Dev. Biol. *17*, 424–432.

Fletcher, M.L., and Wilson, D.A. (2003). Olfactory bulb mitral-tufted cell plasticity: odorant-specific tuning reflects previous odorant exposure. J. Neurosci. *23*, 6946–6955.

Friedrich, R.W., and Korsching, S.I. (1997). Combinatorial and chemotopic odorant coding in the zebrafish olfactory bulb visualized by optical imaging. Neuron *18*, 737–752.

Green, D.M., and Swets, J.A. (1974). Signal Detection Theory and Psychophysics (Huntington, NY: R.E. Krieger Pub. Co.).

Hara, K., and Harris, R.A. (2002). The anesthetic mechanism of urethane: the effects on neurotransmitter-gated ion channels. Anesth. Analg. *94*, 313–318.

Hartline, H.K., Wagner, H.G., and Ratliff, F. (1956). Inhibition in the eye of Limulus. J. Gen. Physiol. *39*, 651–673.

Isaacson, J.S., and Strowbridge, B.W. (1998). Olfactory reciprocal synapses: dendritic signaling in the CNS. Neuron *20*, 749–761.

Johnson, B.A., and Leon, M. (2007). Chemotopic odorant coding in a mammalian olfactory system. J. Comp. Neurol. *503*, 1–34.

Kay, L.M., and Laurent, G. (1999). Odor- and context-dependent modulation of mitral cell activity in behaving rats. Nat. Neurosci. *2*, 1003–1009.

Kuffler, S.W. (1953). Discharge patterns and functional organization of mammalian retina. J. Neurophysiol. *16*, 37–68.

Lin, D.Y., Zhang, S.Z., Block, E., and Katz, L.C. (2005). Encoding social signals in the mouse main olfactory bulb. Nature *434*, 470–477.

Luo, M., and Katz, L.C. (2001). Response correlation maps of neurons in the mammalian olfactory bulb. Neuron *32*, 1165–1179.

Macrides, F., and Chorover, S.L. (1972). Olfactory bulb units: activity correlated with inhalation cycles and odor quality. Science *175*, 84–87.

McLean, J.H., and Shipley, M.T. (1991). Postnatal development of the noradrenergic projection from locus coeruleus to the olfactory bulb in the rat. J. Comp. Neurol. *304*, 467–477.

Meister, M., and Bonhoeffer, T. (2001). Tuning and topography in an odor map on the rat olfactory bulb. J. Neurosci. *21*, 1351–1360.

Mombaerts, P. (2006). Axonal wiring in the mouse olfactory system. Annu. Rev. Cell Dev. Biol. *22*, 713–737.

Mori, K., and Shepherd, G.M. (1994). Emerging principles of molecular signal processing by mitral/tufted cells in the olfactory bulb. Semin. Cell Biol. *5*, 65–74.

Mori, K., Takahashi, Y.K., Igarashi, K.M., and Yamaguchi, M. (2006). Maps of odorant molecular features in the Mammalian olfactory bulb. Physiol. Rev. *86*, 409–433.

Motokizawa, F. (1996). Odor representation and discrimination in mitral/tufted cells of the rat olfactory bulb. Exp. Brain Res. *112*, 24–34.

Nagayama, S., Takahashi, Y.K., Yoshihara, Y., and Mori, K. (2004). Mitral and tufted cells differ in the decoding manner of odor maps in the rat olfactory bulb. J. Neurophysiol. *91*, 2532–2540.

Neville, K.R., and Haberly, L.B. (2003). Beta and gamma oscillations in the olfactory system of the urethane-anesthetized rat. J. Neurophysiol. *90*, 3921–3930.

Olshausen, B.A., and Field, D.J. (2005). How close are we to understanding V1? Neural Comput. *17*, 1665–1699.

Onoda, N., and Mori, K. (1980). Depth distribution of temporal firing patterns in olfactory bulb related to air-intake cycles. J. Neurophysiol. *44*, 29–39.

Orona, E., Rainer, E.C., and Scott, J.W. (1984). Dendritic and axonal organization of mitral and tufted cells in the rat olfactory bulb. J. Comp. Neurol. *226*, 346–356.

Rall, W., and Shepherd, G.M. (1968). Theoretical reconstruction of field potentials and dendrodendritic synaptic interactions in olfactory bulb. J. Neurophysiol. *31*, 884–915.

Ratliff, F., and Hartline, H.K. (1959). The responses of Limulus optic nerve fibers to patterns of illumination on the receptor mosaic. J. Gen. Physiol. *42*, 1241–1255.

Rinberg, D., and Gelperin, A. (2006). Olfactory neuronal dynamics in behaving animals. Semin. Cell Dev. Biol. *17*, 454–461.

Rinberg, D., Koulakov, A., and Gelperin, A. (2006). Sparse odor coding in awake behaving mice. J. Neurosci. *26*, 8857–8865.

Rubin, B.D., and Katz, L.C. (1999). Optical imaging of odorant representations in the mammalian olfactory bulb. Neuron *23*, 499–511.

Scott, J.W. (1981). Electrophysiological identification of mitral and tufted cells and distributions of their axons in olfactory system of the rat. J. Neurophysiol. *46*, 918–931.

Shepherd, G.M., and Greer, C.A. (2004). Olfactory bulb. In The Synaptic Organization of the Brain, G.M. Shepherd, ed. (Oxford, New York: Oxford University Press), pp. 165–216.

Sincich, L.C., and Blasdel, G.G. (2001). Oriented axon projections in primary visual cortex of the monkey. J. Neurosci. *21*, 4416–4426.

Spors, H., and Grinvald, A. (2002). Spatio-temporal dynamics of odor representations in the mammalian olfactory bulb. Neuron *34*, 301–315.

Srinivasan, M.V., Laughlin, S.B., and Dubs, A. (1982). Predictive coding: a fresh view of inhibition in the retina. Proc. R. Soc. Lond. B. Biol. Sci. *216*, 427–459.

Strotmann, J., Conzelmann, S., Beck, A., Feinstein, P., Breer, H., and Mombaerts, P. (2000). Local permutations in the glomerular array of the mouse olfactory bulb. J. Neurosci. *20*, 6927–6938.

Uchida, N., Takahashi, Y.K., Tanifuji, M., and Mori, K. (2000). Odor maps in the mammalian olfactory bulb: domain organization and odorant structural features. Nat. Neurosci. *3*, 1035–1043.

Wachowiak, M., and Cohen, L.B. (2001). Representation of odorants by receptor neuron input to the mouse olfactory bulb. Neuron *32*, 723–735.

Wachowiak, M., and Shipley, M.T. (2006). Coding and synaptic processing of sensory information in the glomerular layer of the olfactory bulb. Semin. Cell Dev. Biol. *17*, 411–423.

Werblin, F.S., and Dowling, J.E. (1969). Organization of the retina of the mudpuppy, Necturus maculosus. II. Intracellular recording. J. Neurophysiol. *32*, 339–355.

Willhite, D.C., Nguyen, K.T., Masurkar, A.V., Greer, C.A., Shepherd, G.M., and Chen, W.R. (2006). Viral tracing identifies distributed columnar organization in the olfactory bulb. Proc. Natl. Acad. Sci. USA *103*, 12592–12597.

Willmore, B., and Smyth, D. (2003). Methods for first-order kernel estimation: simple-cell receptive fields from responses to natural scenes. Network *14*, 553–577.

Yokoi, M., Mori, K., and Nakanishi, S. (1995). Refinement of odor molecule tuning by dendrodendritic synaptic inhibition in the olfactory bulb. Proc. Natl. Acad. Sci. USA *92*, 3371–3375.

Yoshioka, T., Blasdel, G.G., Levitt, J.B., and Lund, J.S. (1996). Relation between patterns of intrinsic lateral connectivity, ocular dominance, and cytochrome oxidase-reactive regions in macaque monkey striate cortex. Cereb. Cortex *6*, 297–310.

Neuron, Volume 59

Supplemental Data

Rat Olfactory Bulb Mitral Cells Receive Sparse Glomerular Inputs

Antoniu L. Fantana, Edward R. Soucy, and Markus Meister

Figure S1. Response prediction under varying signal detection thresholds

We varied the thresholds for detecting an odor response among glomeruli (A) or among mitral cells (C), and evaluated the resulting predictions for the responsivity of mitral cells (B and D), using the methods of Figure 6 and an integration radius of 880 μm.

(A) Left: Sample intrinsic image of an odor response. (i) The same image clipped with the threshold value obtained from ROC analysis in Figure 5; most bona fide glomerular responses are detected properly with this threshold. (ii) Same image clipped with the threshold that would be required to match the observed number of effective odors in mitral cells; in this case many obvious responses in glomeruli get suppressed.

(B) The predicted number of effective odors for a mitral cell, plotted against the detection threshold for glomerular signals. Open circle: threshold value derived from ROC analysis in Figure 5; all thresholds are normalized to this value. Closed circle: threshold that would be required to match the observed number of effective odors in mitral cells (mean of “actual” distribution in Figure 6B). This exceeds by more than 3-fold the reasonable value from ROC analysis (open circle).

(C) A sample mitral cell recording. The firing patterns were analyzed as in Figure 3B, and different thresholds applied. (i) Gray bars denote odor responses that exceed the threshold value chosen by ROC analysis in Figure 4; the sole bona fide response in this segment is detected correctly at this threshold. (ii) odor responses that exceed the threshold required to match the

predicted number of effective odors in Figure 6; this accepts many firing patterns as responses that are indistinguishable from air control stimuli.

(D) The number of effective odors for a mitral cell, plotted against the detection threshold for mitral cell responses. Open circle: detection threshold derived from ROC analysis (Figure 4); all thresholds are normalized to this value. Closed circle: detection threshold that would be required to match the predicted number of effective odors in mitral cells (mean of "predicted" distribution in Figure 6B). This is more than 3-fold lower than the reasonable value from ROC analysis (open circle).

Figure S2. Mitral cell odor spectra and their component glomerular spectra

We modeled the response of a mitral cell by a linear weighted sum of responses from 4 glomeruli (Figure 8, Equations 3 and 6). Top: For the 3 mitral cells from Figure 8i-iii, this illustrates the odor spectra of the 4 chosen glomeruli, each scaled by the corresponding connection strength, w_i in Equation 3. Bottom: The predicted spectrum of the mitral cell (sum of the 4 spectra at top) and the actual observed spectrum (2 repeats).

Table 1. List of all odors.

An alphabetic list of the 63 odors used in this report, along with the number of glomeruli activated per bulb (average of 6 bulbs). Some odors were used too infrequently for a reliable assessment of the number of glomeruli.

Table 2. Lookup table for odor axes in figures.

The first column lists the number that appears on the odor axis in various figures. The other 3 columns contain the corresponding odor. The 40 odors in List A were used in the vast majority of experiments performed, including Figures 5A, 8Biii, 8Biv. List B is for Figure 8Bii. List C is for Figures 7B, 7C, 8Bi.

Figure S1

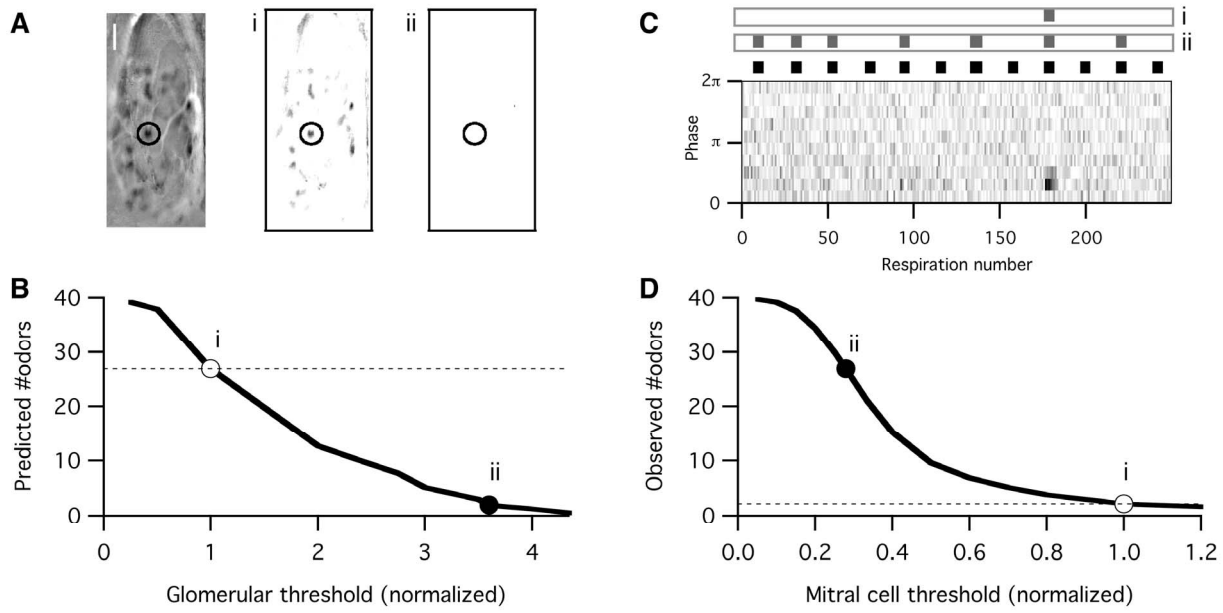

Figure S2

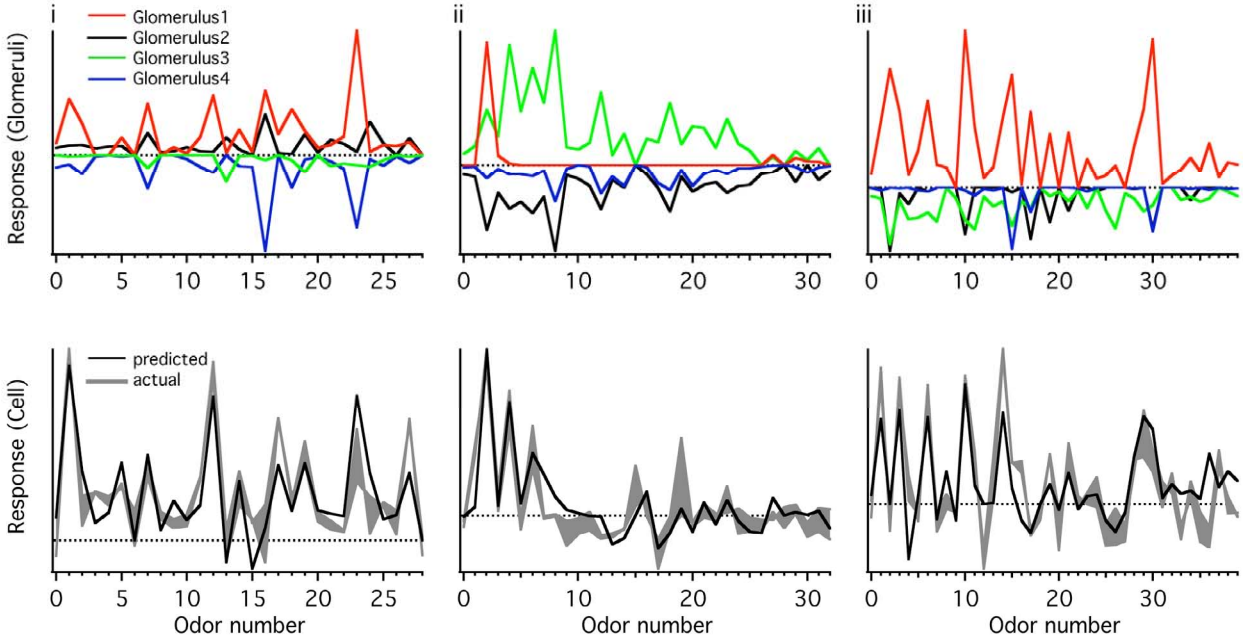

Table S1

Odor Name	Glomeruli
1-butanol	
2,3-diethylpyrazine	
2-ethoxy thiazole	4.3
2-heptanone	20.8
2-hexanone	
2-hexenal	9.3
2-isobutyl thiazole	12.0
2-methyl 3-ethyl pyrazine	1.5
3-acetyl 2,5-dimethyl furan	1.5
3-hexanone	12.8
3-methyl pyrazine	
4-heptanone	17.0
4-methoxyacetophenone	
butyl acetate	10.5
butyl formate	5.0
butyl sulfide	
butyraldehyde	5.0
butyric acid	
camphor	
cineole	1.3
citral	1.2
citronellal	4.5
cyclohexylacetate	3.5
ethyl 2-methyl butyrate	2.5
ethyl butyrate	14.0
ethyl hexanoate	10.5
ethyl octanoate	0.5
ethyl valerate	
fencone	
furfuryl hexanate	
ginger	
heptanal	
heptanoic acid	
heptanol	
hexanal	
hexanoic acid	1.3
hexanol	1.2
hexyl butyrate	2.3
hexyl tiglate	1.8
isoamyl acetate	13.5
isoamylamine	0.7
isobutyl proprionate	21.0
isopropyl butyrate	
lemon	
methoxy pyrazine	0.8
methyl butyrate	8.5
methyl tiglate	14.0
mineral oil	0.0
nonanal	3.2
nonanoic acid	1.2
nonanol	3.8
nutmeg	
octanal	11.8
octanoic acid	0.2
octanol	6.5
pentanol	
peppermint (10%)	5.5
pine	
propyl tiglate	5.5
pyrrolidine	0.7
valeraldehyde	4.5
valeric acid	0.7
verenone	

Table S2

Odor Number	Odor Name		
	List A	**List B**	**List C**
0	mineral oil	mineral oil	mineral oil
1	peppermint (10%)	peppermint (10%)	peppermint (10%)
2	methyl tiglate	methyl tiglate	butyraldehyde
3	ethyl butyrate	propyl tiglate	butyric acid
4	methyl butyrate	ethyl valerate	pentanol
5	butyraldehyde	isobutyl proprionate	valeric acid
6	propyl tiglate	ethyl hexanoate	hexanol
7	valeraldehyde	isopropyl butyrate	ethyl hexanoate
8	valeric acid	2,3-diethylpyrazine	hexanal
9	hexanol	hexanoic acid	hexanoic acid
10	isobutyl proprionate	heptanol	heptanol
11	ethyl hexanoate	hexyl tiglate	hexyl tiglate
12	hexanoic acid	2-isobutyl thiazole	hexyl butyrate
13	hexyl tiglate	2-heptanone	2-heptanone
14	hexyl butyrate	octanol	heptanal
15	2-isobutyl thiazole	ethyl octanoate	heptanoic acid
16	2-heptanone	3-hexanone	octanol
17	octanol	octanal	2-hexanone
18	ethyl octanoate	2-hexenal	3-hexanone
19	3-hexanone	citronellal	octanal
20	isoamylamine	isoamyl acetate	octanoic acid
21	2-ethoxy thiazole	4-heptanone	nonanol
22	citral	nutmeg	2-hexenal
23	octanal	ginger	4-heptanone
24	octanoic acid	lemon	nonanal
25	nonanol	pine	nonanoic acid
26	2-hexenal	fencone	1-butanol
27	pyrrolidine	butyl sulfide	3-methyl pyrazine
28	citronellal	verenone	furfuryl hexanate
29	isoamyl acetate	ethyl 2-methyl butyrate	
30	4-heptanone	butyl acetate	
31	nonanal	camphor	
32	nonanoic acid	4-methoxyacetophenone	
33	cineole		
34	3-acetyl 2,5-dimethyl furan		
35	butyl formate		
36	cyclohexylacetate		
37	butyl acetate		
38	2-methyl 3-ethyl pyrazine		
39	methoxy pyrazine		